Emergent conservation in the Floquet dynamics of integrable non-Hermitian models

Tista Banerjee and K. Sengupta

School of Physical Sciences, Indian Association for the Cultivation of Science, Jadavpur, Kolkata 700032, India

(Received 27 October 2022; revised 3 February 2023; accepted 21 March 2023; published 10 April 2023)

We study the dynamics of a class of integrable non-Hermitian free-fermionic models driven periodically using a continuous drive protocol characterized by an amplitude g_1 and frequency ω_D. We derive an analytic, albeit perturbative, Floquet Hamiltonian for describing such systems using Floquet perturbation theory with g_1^{-1} being the perturbation parameter. Our analysis indicates the existence of special drive frequencies at which an approximately conserved quantity emerges. The presence of such an almost conserved quantity is reflected in the dynamics of the fidelity, the correlation functions, and the half-chain entanglement entropy of the driven system. In addition, it also controls the nature of the steady state of the system. We show that one-dimensional transverse field Ising model, with an imaginary component of the transverse field, serves as an experimentally relevant example of this phenomenon. In this case, the transverse magnetization is approximately conserved; this conservation leads to complete suppression of oscillatory features in the transient dynamics of fidelity, magnetization, and entanglement of the driven chain at special drive frequencies. We discuss the nature of the steady state of the Ising chain near and away from these special frequencies, demonstrate the protocol independence of this phenomenon by showing its existence for discrete drive protocols, and suggest experiments which can test our theory.

DOI: 10.1103/PhysRevB.107.155117

I. INTRODUCTION

The study of nonequilibrium dynamics of closed quantum systems has received tremendous theoretical [1–9] and experimental [10–14] attention in recent years. Of the several protocols available to drive a system out of equilibrium, periodic drive protocols have been studied most intensely. The evolution operator U for such periodically driven systems at stroboscopic times $t = nT$, where $T = 2\pi/\omega_D$ is the time period of the drive, n is an integer, and ω_D is the drive frequency, can be expressed in terms of its Floquet Hamiltonian H_F as [9,15]

$$U(nT, 0) = \exp[-iH_F nT/\hbar]. \tag{1}$$

The study of such driven systems therefore amounts to analysis of their Floquet Hamiltonian.

The theoretical focus on periodically driven closed quantum systems is mostly due to the fact that they display various features that have no analog in their aperiodic counterparts. Some of these include generation of topologically nontrivial Floquet states [16–20], realization of time crystals [21–23], and tuning ergodicity properties of nonintegrable quantum systems [24–26]. In addition, they host phenomena such as dynamical transitions [27–29], dynamical localization [30–32], and dynamical freezing [25,26,33–37].

More recently, there has been considerable interest in study of non-Hermitian quantum Hamiltonians [38–51]. Such Hamiltonians may provide effective description for open quantum systems [52]. In addition, they display several interesting features such as non-Hermitian skin effect [53–55], phase transition related to explicit breaking of PT symmetry [38], and the presence of exceptional points where two or more complex eigenvalues of a such Hamiltonians coincide and corresponding eigenstates coalesce [38]. The presence of such exceptional points leads to unconventional topological features and novel bulk-edge correspondence in these systems which have no analog in systems described by Hermitian quantum Hamiltonians [56–60].

The description of out-of-equilibrium dynamics of such non-Hermitian quantum systems has also been carried out [61–66]. Most of these studies concentrated on periodically driven systems and can be classified into two distinct groups. The first involves study of systems driven using continuous protocols at high frequencies where Magnus expansion may be used to obtain analytic insight [63]. The second involves use of discrete drive protocols where exact solution of the Floquet Hamiltonian is available for integrable non-Hermitian models [61,62]. Such studies has led to several interesting phenomena such as non-Hermitian analog of Floquet dynamical transitions [61], optically induced Liftshitz transition in non-Hermitian Weyl semimetals [63], drive-induced PT symmetry breaking [62], and non-Hermitian topological phases and transitions [61]. In addition, quench dynamics of non-Hermitian quantum spin chains has also been studied with focus on time evolution of correlation and entanglement entropy of such a chain following the quench [65].

In this work we study the periodic dynamics of a non-Hermitian free-fermionic integrable model whose Hamiltonian is given by

$$H = \sum_{\vec{k}} \psi_{\vec{k}}^{\dagger}(\tau_3(g + i\gamma - a_{3\vec{k}}) + \Delta_{\vec{k}}\tau_1)\psi_{\vec{k}}, \tag{2}$$

where $\psi_{\vec{k}}$ is a two-component fermion field and $\vec{\tau} = (\tau_1, \tau_2, \tau_3)$ denotes corresponding Pauli matrices. Here g, $a_{3\vec{k}}$, and $\Delta_{\vec{k}}$ are parameters of the model, and the presence of $\gamma > 0$ makes the model non-Hermitian. The Hermitian counterparts ($\gamma = 0$) class of models serves as prototype for a study of wide range of condensed matter system; in $d = 1$, it represents Ising and XY spin models [67]. For these models, $a_{3k} = 2\cos k$, $\Delta_k = 2\sin k$, and the two component field $\psi_k = (c_k, c^{\dagger}_{-k})^T$, where c_k denote fermion annihilation operator. In $d = 2$, $H(\gamma = 0)$ describes the physics of Dirac quasiparticles in graphene [68] and on surfaces of topological insulators [69], as well as the fermionic description of the Kitaev honeycomb model [70]. Finally, in $d = 3$, the model can be used to describe quasiparticles in Weyl semimetals [71].

The presence of a nonzero γ leads to non-Hermitian nature of the model. One context in which such a term naturally appears is the one-dimensional (1D) Ising model in the presence of a measuring operator which measures $\hat{n}_j = (1 - \sigma^z_j)/2$ (where σ^z_j denotes the usual Pauli matrix representing the spin on site j of the chain) with a rate γ and in the so-called no-click limit [65,72,73]; this leads to a complex magnetic field term in the effective Hamiltonian of the spin chain [65]. Similar models of non-Hermitian chains have been discussed in different contexts as well [74,75]. In the present manuscript, we shall assume the existence of such nonhermiticity and study the Floquet dynamics of the resultant model. We note in this context that the quench dynamics of such a model has already been studied in Ref. [65].

The main results that we obtain from our study are as follows. First, we obtain an perturbative Floquet Hamiltonian, using Floquet perturbation theory (FPT), which reproduces all qualitative features of the dynamics of the model and provide analytical insight into emergence of approximate conserved quantities in this system. The FPT uses inverse of the drive amplitude as the perturbation parameter; it produces qualitatively accurate results both in high and intermediate drive frequency regime where a standard high-frequency expansion fails [9].

Second, using the FPT, we identify special frequencies at which the first-order Floquet Hamiltonian of the system, $H_F^{(1)}$ leads to conserved quantities, i.e., $[H_F^{(1)}, \hat{O}] = 0$ for a specific operator $\hat{O}$. An example of such an operator, as we shall show, is the transverse magnetization of the Ising chain. Such a conservation is approximate since it is violated by higher order terms in the Floquet Hamiltonian. Nevertheless, we show, that the approximate conservation leaves distinct imprint on the dynamics of the system which turns out to be qualitatively different near and away from these special frequencies. We also demonstrate the protocol-independence of this phenomenon by demonstrating its presence for the discrete square pulse protocol.

Third, we find that at these special frequencies, the correlation functions, fidelity, and entanglement entropy shows distinct lack of transient oscillations provided one starts from an eigenstate of the conserved operator $\hat{O}$. The absence of such oscillations, which are typically present when the drive frequency is different from the special frequencies, can be directly linked to the approximate conservation mentioned above. Moreover, the steady state of the driven system turns out to be close to an eigenstate of the nearly conserved operator for any chosen initial state. For example, consider the non-Hermitian Ising model whose Hamiltonian is given by

$$H_{\rm Ising} = -J\left(\sum_{\langle ij\rangle} \sigma^x_i \sigma^x_j + (h(t) + i\gamma)\sum_j \sigma^z_j\right), \qquad (3)$$

where J s the interaction strength, σ^x_j and σ^z_j denote Pauli matrices on site j, and $h(t) = h_0 + h_1 \cos\omega_D t$ denotes the time-dependent dimensionless transverse field. The transverse magnetization of this Ising chain is given by $S_z = \sum_j \sigma^z_j$. At these special frequencies S_z is almost conserved and the steady state, for $\gamma > 0$, is close to the ferromagnetic state with all spins up (eigenstate of σ^z_j with eigenvalue 1). Moreover, the magnetization dynamics, starting from all spin-down state, show complete absence of transient oscillations which are normally present at other drive frequencies. Thus, our results show that the emergent approximate conservation law in such driven system leaves its imprint on both the dynamics and the steady-state values of experimentally accessible quantities such as magnetization of the Ising model. To the best of our knowledge, this phenomenon has not been pointed out earlier in the literature.

The organization of the rest of the paper is as follows. In Sec. II, we demonstrate the emergence of conserved quantities via derivation of the Floquet Hamiltonian corresponding to driven free fermionic systems. We also provide semianalytic expressions of fidelity, correlation functions, and entanglement entropy for the driven model. This is followed by Sec. III where we present our numerical results for the 1D transverse field Ising model demonstrating qualitative match between results obtained from FPT and exact numerics. Finally, in Sec. IV, we discuss our main results, suggest possible experiments which can test our theory, and conclude. The presence of similar emergence of approximate conserved quantities for discrete drive protocol is discussed in the Appendix.

II. FLOQUET PERTURBATION THEORY

In this section, we provide an analytic, albeit perturbative expression of the Floquet Hamiltonian of the driven integrable non-Hermitian model given by Eq. (2) using Floquet perturbation theory. The protocol that we use is given by

$$g(t) = g_0 + g_1 \cos\omega_D t, \qquad (4)$$

where g_0 is the static part of the drive and g_1 is the drive amplitude. We compute the Floquet Hamiltonian in Sec. II A. This is followed by analytic expressions of correlation function, fidelity, entanglement entropy for the driven model in Sec. II B.

A. Perturbative Floquet Hamiltonian

In the presence of the drive given by Eq. (4), the Floquet Hamiltonian corresponding to Eq. (2) cannot be computed exactly. This is in contrast to discrete protocols studied in the literature [61,62]. To obtain an analytic understanding, we therefore use the Floquet perturbation theory to compute H_F in the regime where $g_1 \gg g_0, |\Delta_{\vec{k}}|, |a_{3\vec{k}}|$. In this regime, one

can write the Hamiltonian as $H_{\vec{k}} = H_{0\vec{k}} + H_{1\vec{k}}$, where

$$H_{0\vec{k}} = \tau_3 g_1 \cos\omega_D t,$$
$$H_{1\vec{k}} = \tau_3(g_0 + i\gamma - a_{3\vec{k}}) + \tau_1\Delta_{\vec{k}}. \quad (5)$$

In what follows we shall treat $H_{1\vec{k}}$ perturbatively using FPT [9]. This is usually done by first obtaining the evolution operator $U_0(t,0)$ corresponding to $H_0(t)$ (the term with the largest amplitude in H) exactly; this is followed by computations $U_1, U_2 ... U_n$ which are higher (nth)-order corrections to U_0 due to H_1. One can then use these perturbative evolution operators U_n to obtain the nth-order Floquet Hamiltonian [9]. In what follows, we shall restrict ourselves to the first- and second-order perturbative corrections.

We begin by computing the evolution operator which, to zeroth order in g_1, is given by

$$U_{0\vec{k}}(t,0) = e^{-i\int_0^t H_{0\vec{k}}dt'/\hbar} = \exp\left[-i\tau_3\frac{g_1\sin\omega_D t}{\hbar\omega_D}\right]. \quad (6)$$

Thus, $U_{0\vec{k}}(T,0) = I$ (where I denotes the 2×2 identity matrix) and $H^{(0)}_{F\vec{k}} = 0$ for all $\vec{k}$. Note that the expression of $U_{0\vec{k}}(t,0)$ is derived using the fact that $H_{0\vec{k}}(t)$ commutes with itself at all times.

The first-order Floquet Hamiltonian can be constructed using standard perturbation theory. To this end, we first write the expression of $U_{1\vec{k}}(T,0)$ which is given by

$$U_{1\vec{k}}(T,0) = \frac{-i}{\hbar}\int_0^T dt\; U^\dagger_{0\vec{k}}(t,0)H_{1\vec{k}}U_{0\vec{k}}(t,0)$$
$$= \frac{-iT}{\hbar}\left[\tau_3(g_0 + i\gamma - a_{3\vec{k}}) + \tau_1\Delta_{\vec{k}}J_0\left(\frac{2g_1}{\hbar\omega_D}\right)\right], \quad (7)$$

where $J_0(x)$ denotes the zeroth-order Bessel function. Note that the first term in Eq. (7) follows trivially since $U_0(t,0)$ commutes with τ_3 at all times. The computation of the second term can be done in a straightforward manner using the relation $\tau_x U_{0\vec{k}}(t,0) = U^\dagger_{0\vec{k}}(t,0)\tau_x$ and the identity $\exp[ia\sin x] = \sum_{n=-\infty}^{\infty} J_n(a)\exp[inx]$. Using Eq. (7), we find that the first-order Floquet Hamiltonian is given by

$$H^{(1)}_{F\vec{k}} = \frac{i\hbar}{T}U_{1\vec{k}}(T,0)$$
$$= \tau_3(\alpha_{\vec{k}} + i\gamma) + \tau_1\Delta_{\vec{k}}J_0\left(\frac{2g_1}{\hbar\omega_D}\right), \quad (8)$$

where $\alpha_{\vec{k}} = g_0 - a_{3\vec{k}}$.

We note that at special frequencies, for a fixed drive amplitude, which satisfy $2g_1/(\hbar\omega^*_m) = \rho_m$ where ρ_m denotes the position of the mth zero of J_0, the off-diagonal term of $H^{(1)}_{F\vec{k}}$ vanishes for all $\vec{k}$. At these frequencies, $[H^{(1)}_{F\vec{k}}, \tau_3] = 0$. This constitutes an emergent dynamical symmetry which forces the dynamics to conserve τ_3 for all $\vec{k}$. This symmetry will be broken by higher order terms in the Floquet Hamiltonian as we shall show later in this section. However, we note that at large drive frequencies, the contribution of the higher order Floquet Hamiltonian are small and we shall see that the correlation functions of the driven system bear signature of this approximate dynamical symmetry. The presence of similar special frequencies for discrete square pulse protocol has been shown in the Appendix.

Next we compute the second-order Floquet Hamiltonian. To this end, we first note that the second-order evolution operator $U_{2\vec{k}}(T,0)$ is given by

$$U_{2\vec{k}}(T,0) = \left(\frac{-i}{\hbar}\right)^2\int_0^T dt_1\; U^\dagger_{0\vec{k}}(t_1,0)H_{1\vec{k}}U_{0\vec{k}}(t_1,0)\int_0^{t_1} dt_2\; U^\dagger_{0\vec{k}}(t_2,0)H_{1\vec{k}}U_{0\vec{k}}(t_2,0)$$
$$= \left(\frac{-i}{\hbar}\right)^2\int_0^T dt_1\int_0^{t_1} dt_2\begin{pmatrix}(\alpha_{\vec{k}}+i\gamma)^2 + A_{\vec{k}}(t_1,t_2) & (\alpha_{\vec{k}}+i\gamma)B_{\vec{k}}(t_1,t_2)\\ -(\alpha_{\vec{k}}+i\gamma)B^*_{\vec{k}}(t_1,t_2) & (\alpha_{\vec{k}}+i\gamma)^2 + A^*_{\vec{k}}(t_1,t_2)\end{pmatrix}, \quad (9)$$

where the functions $A_{\vec{k}}(t_1,t_2)$ and $B_{\vec{k}}(t_1,t_2)$ are given by

$$A_{\vec{k}}(t_1,t_2) = \Delta^2_{\vec{k}}e^{\frac{2ig_1}{\hbar\omega_D}(\sin\omega_D t_1 - \sin\omega_D t_2)},$$
$$B_{\vec{k}}(t_1,t_2) = \Delta_{\vec{k}}\left(e^{\frac{2ig_1}{\hbar\omega_D}\sin\omega_D t_2} - e^{\frac{2ig_1}{\hbar\omega_D}\sin\omega_D t_1}\right). \quad (10)$$

The integrations can be easily carried out using standard identities involving Bessel functions. A straightforward computation leads to the second-order Floquet Hamiltonian

$$H^{(2)}_{F\vec{k}} = \frac{i\hbar}{T}\left(U_{2\vec{k}}(T,0) - U^2_{1\vec{k}}(T,0)/2\right) = -\tau_3 4\Delta^2_{\vec{k}}\sum_{n=0}^{\infty}\frac{J_0\left(\frac{2g_1}{\hbar\omega_D}\right)J_{2n+1}\left(\frac{2g_1}{\hbar\omega_D}\right)}{(2n+1)\hbar\omega_D} + \tau_1 4\Delta_{\vec{k}}(\alpha_{\vec{k}} + i\gamma)\sum_{n=0}^{\infty}\frac{J_{2n+1}\left(\frac{2g_1}{\hbar\omega_D}\right)}{(2n+1)\hbar\omega_D}. \quad (11)$$

Combining Eqs. (8) and (11), we find the final Floquet Hamiltonian to be

$$H_{F\vec{k}} = \tau_3 S_{1\vec{k}} + \tau_1 S_{2\vec{k}}, \quad S_{1\vec{k}} = (\alpha_{1\vec{k}} + i\gamma),$$
$$\alpha_{1\vec{k}} = \alpha_{\vec{k}} - 2\Delta^2_{\vec{k}}\sum_{n=0}^{\infty}\frac{J_0\left(\frac{2g_1}{\hbar\omega_D}\right)J_{2n+1}\left(\frac{2g_1}{\hbar\omega_D}\right)}{(n+1/2)\hbar\omega_D}, \quad S_{2\vec{k}} = \Delta_{\vec{k}}(\alpha_{2\vec{k}} + i\gamma\lambda),$$
$$\alpha_{2\vec{k}} = \left(J_0\left(\frac{2g_1}{\hbar\omega_D}\right) + \alpha_{\vec{k}}\lambda\right), \quad \lambda = 2\sum_{n=0}^{\infty}\frac{J_{2n+1}\left(\frac{2g_1}{\hbar\omega_D}\right)}{(n+1/2)\hbar\omega_D}. \quad (12)$$

The energy spectrum of the Floquet Hamiltonian can be easily found by diagonalizing $H_{F\vec{k}}$. We find two energy bands whose expressions are given by

$$\begin{aligned} E^{\pm}_{\vec{k}} &= \pm E_{\vec{k}}; \quad E_{\vec{k}} = (\epsilon_{\vec{k}} + i\Gamma_{\vec{k}}), \\ \epsilon_{\vec{k}} &= \frac{1}{\sqrt{2}}\sqrt{\beta_1 + \sqrt{\beta_1^2 + 4\gamma^2(\alpha_1 + \Delta_{\vec{k}}\alpha_2\lambda)^2}}, \\ \Gamma_{\vec{k}} &= \frac{\gamma\left(\alpha_1 + \Delta^2_{\vec{k}}\alpha_2\lambda\right)}{\epsilon_{\vec{k}}}, \\ \beta_1 &= \alpha_1^2 + \Delta^2_{\vec{k}}\alpha_2^2 - \gamma^2\left(1 + \Delta^2_{\vec{k}}\lambda^2\right), \end{aligned} \tag{13}$$

where we have not written down the $\vec{k}$ dependence of α_1, β_1, and α_2 defined in Eq. (12) for brevity.

We note that the Floquet quasienergy spectrum allows for long-lived quasienergy excitations for $\vec{k} = \vec{k}_0$ which satisfies $\alpha_{1\vec{k}_0} = -\lambda\Delta^2_{\vec{k}_0}\alpha_{2\vec{k}_0}$. Furthermore, it also shows the presence of exceptional point for a critical $\gamma = \gamma_E$ such that

$$\gamma_E = \pm\Delta_{\vec{k}_0}\alpha_{2\vec{k}_0}. \tag{14}$$

It is easy to check that at these points $E^{\pm}_{\vec{k}_0} = 0$.

Thus, the perturbative Floquet theory predicts that the position of both long-lived quasienergy modes and the presence/absence of exceptional points can be tuned using the amplitude and frequency of the drive. In the next section, we shall see that this statement holds qualitatively for the exact spectrum. We note that the second-order Hamiltonian $H^{(2)}_{F\vec{k}}$ leads to smaller contribution at large frequencies since its terms are suppressed by a overall factor of $1/\omega_D$. However, its contribution to $H_{F\vec{k}}$ becomes important near special frequencies ω^*_m for which $J_0[2g_1/(\hbar\omega^*_m)] = 0$. At these frequencies $H^{(2)}_{F\vec{k}}$ contributes the only nonzero off-diagonal term in $H_{F\vec{k}}$ (up to second-order perturbation theory) and its inclusion is therefore crucial to obtain a qualitative match of the perturbative analytical results with exact numerics.

B. Correlators, entanglement, and fidelity

In this section, we shall express the correlation functions, fidelity, and entanglement entropy of the driven integrable model in terms of the eigenvalues and eigenvectors of $H_{F\vec{k}}$. This will be particularly helpful in deducing their properties using the expressions of second-order Floquet energy derived in Eq. (12).

We start by noting that the normalized eigenvectors of the second-order Floquet Hamiltonian corresponding to Floquet energies $E^{\pm}_{\vec{k}}$ can be expressed in terms of components of a unit vector $\vec{n}_{\vec{k}} = (n_{x\vec{k}}, 0, n_{z\vec{k}})$, where

$$n_{x\vec{k}} = S_{2\vec{k}}/E_{\vec{k}}, \quad n_{z\vec{k}} = S_{1\vec{k}}/E_{\vec{k}}. \tag{15}$$

In terms of these, the normalized eigenvectors of $H_{F\vec{k}}$ corresponding to quasienergies $\pm E_{\vec{k}}$ are given by

$$\begin{aligned} |\pm;\vec{k}\rangle &= \frac{1}{\mathcal{N}_{\pm\vec{k}}}\begin{pmatrix} p_{\pm\vec{k}} \\ q_{\pm\vec{k}} \end{pmatrix} \quad p_{\pm\vec{k}} = n_{z\vec{k}} \pm 1, \\ q_{\pm\vec{k}} &= n_{x\vec{k}} \quad \mathcal{N}_{\pm\vec{k}} = \sqrt{|n_{z\vec{k}} \pm 1|^2 + |n_{x\vec{k}}|^2}. \end{aligned} \tag{16}$$

Note that for $|g_0| \leqslant 2$, $\Gamma_{\vec{k}} = \mathrm{Im}[E_{\vec{k}}]$ changes sign across $\vec{k} = \vec{k}^*$ for which $\alpha_{1\vec{k}^*} = -\alpha_{2\vec{k}^*}\lambda\Delta^2_{\vec{k}^*}$. In this case, for $\omega_D \simeq \omega^*_m$ where $S_{2\vec{k}}/E_{\vec{k}} \ll 1$ for all $\vec{k}$, and for $\gamma > 0$, the eigenfunction of $H_{F\vec{k}}$ corresponding to $\Gamma_{\vec{k}} > 0$ changes from $\sim(0,1)^T$ to $\sim(1,0)^T$ sharply as one crosses $\vec{k}^*$. In contrast, such a change is much more gradual away from the special frequencies where $S_{2\vec{k}}/E_{\vec{k}}$ is not small.

In terms of $|\pm;\vec{k}\rangle$, it is possible to write the evolution operator of the system at stroboscopic times $t_n = nT$ as

$$U_{\vec{k}}(nT, 0) = \sum_{a=\pm} e^{-iaE_{\vec{k}}nT/\hbar}|a;\vec{k}\rangle\langle a;\vec{k}|. \tag{17}$$

We note that the evolution operator $U_{\vec{k}}(nT, 0)$ is not unitary due to nonzero $\Gamma_{\vec{k}}$. Consequently, to obtain the state after n drive cycles, we need to adapt the standard normalization procedure for non-Hermitian systems [61–65] which yields

$$\begin{aligned} |\psi_{\vec{k}}(nT)\rangle &= \frac{|\tilde{\psi}_{\vec{k}}(nT)\rangle}{|\langle\tilde{\psi}_{\vec{k}}(nT)|\tilde{\psi}_{\vec{k}}(nT)\rangle|}, \\ |\tilde{\psi}_{\vec{k}}(nT)\rangle &= U_{\vec{k}}(nT, 0)|\psi_{0\vec{k}}\rangle, \end{aligned} \tag{18}$$

where $|\psi_{0\vec{k}}\rangle$ is the initial state. In what follows, we shall parametrize the initial state $|\psi_{0\vec{k}}\rangle = (u_{0\vec{k}}, v_{0\vec{k}})^T$ using an angle $\theta_{0\vec{k}}$ such that $u_{0\vec{k}} = \cos\theta_{0\vec{k}}$ and $v_{0\vec{k}} = \sin\theta_{0\vec{k}}$. This allows us to write, using Eqs. (16), (17), and (18), $|\psi_{\vec{k}}(nT)\rangle = (u_{\vec{k}}(nT), v_{\vec{k}}(nT))^T$, where

$$\begin{aligned} u_{\vec{k}}(nT) &= \frac{\sum_{a=\pm} e^{-iaE_{\vec{k}}nT/\hbar}\mu_{a\vec{k}}p_{a\vec{k}}}{\mathcal{D}_{\vec{k}}(\theta_{0\vec{k}})}, \\ v_{\vec{k}}(nT) &= \frac{\sum_{a=\pm} e^{-iaE_{\vec{k}}nT/\hbar}\mu_{a\vec{k}}q_{a\vec{k}}}{\mathcal{D}_{\vec{k}}(\theta_{0\vec{k}})}, \\ \mathcal{D}_{\vec{k}}(\theta_{0\vec{k}}) &= \Bigg[\left|\sum_{a=\pm} e^{-iE_{a\vec{k}}nT/\hbar}p_{a\vec{k}}\mu_{a\vec{k}}\right|^2 \\ &\quad + \left|\sum_{a=\pm} e^{-iE_{a\vec{k}}nT/\hbar}q_{a\vec{k}}\mu_{a\vec{k}}\right|^2\Bigg]^{1/2}, \\ \mu_{\pm\vec{k}} &= p^*_{\pm\vec{k}}\cos\theta_{0\vec{k}} + q^*_{\pm\vec{k}}\sin\theta_{0\vec{k}}. \end{aligned} \tag{19}$$

Using this wave function, one can define the fidelity $\chi(nT) = \prod_{\vec{k}}\chi_{\vec{k}}(nT)$ where $\chi_{\vec{k}}(nT) = |\langle\psi_{0\vec{k}}|\psi_{\vec{k}}(nT)\rangle|^2$. In what follows, we shall be mainly interested in studying the behavior of $g(nT) = \ln\chi(nT)$ [76]. Using Eqs. (18) and (19), one can express $g(nT)$ as

$$g(nT) = \int \frac{d^dk}{V_0}\ln|u_{\vec{k}}(nT)\cos\theta_{0\vec{k}} + v_{\vec{k}}(nT)\sin\theta_{0\vec{k}}|^2, \tag{20}$$

where $V_0 = (2\pi)^d/2$ denotes the volume of the d-dimensional Brillouin zone.

Next, we compute the correlation functions of the model. For the class of integrable models discussed here, the nontrivial correlation functions are given by

$$\begin{aligned} N_{\vec{k}}(nT) &= \langle(2c^\dagger_{\vec{k}}c_{\vec{k}} - 1)\rangle = 2|v_{\vec{k}}(nT)|^2 - 1, \\ F_{\vec{k}}(nT) &= \langle c_{\vec{k}}c_{-\vec{k}} + \mathrm{H.c.}\rangle = (u^*_{\vec{k}}(nT)v_{\vec{k}}(nT) + \mathrm{H.c.}). \end{aligned} \tag{21}$$

The real-space correlation functions can be obtained via Fourier transforms of $N_{\bar{k}}(nT)$ and $F_{\bar{k}}(nT)$.

Finally, we note that for this class of integrable models the entanglement entropy can be expressed in terms of the correlation matrix $\mathcal{C}$. For a 1D fermionic chain of length L and a subsystem of size $\ell \leqslant L$, the correlation matrix can be written as [65]

$$\mathcal{C} = \begin{pmatrix} \Pi_0 & \Pi_{-1} & .. & \Pi_{1-\ell} \\ \Pi_1 & \Pi_0 & .. & \Pi_{2-\ell} \\ .. & .. & .. & .. \\ \Pi_{\ell-1} & \Pi_{\ell-2} & .. & \Pi_0 \end{pmatrix}, \quad \Pi_{\ell_0} = \int \frac{d^d k}{V_0} e^{ik\ell_0} \hat{\Pi}_k \cdot \hat{\tau}_k,$$

$$\Pi_{yk} = 2|v_k(nT)|^2 - 1, \quad \Pi_{xk} = 2\,\mathrm{Re}[u_k(nT)v_k^*(nT)], \quad \Pi_{zk} = 2\,\mathrm{Im}[u_k(nT)v_k^*(nT)]. \tag{22}$$

The entanglement entropy can then be computed using eigenvalues $\zeta_r(nT)$, where $r = 1..2\ell$, of $\mathcal{C}$. In terms of these one obtain the von-Neumann entropy as

$$S_\ell(nT) = -\sum_{r=1}^{2\ell} \zeta_r(nT) \ln \zeta_r(nT). \tag{23}$$

We shall use these expressions to compute the correlations, fidelity, and entanglement both from exact numerics and using the second-order perturbative Floquet Hamiltonian for the 1D Ising chain in the next section.

III. NUMERICAL RESULTS

In this section, we present our numerical results for the driven, non-Hermitian 1D Ising chain with the Hamiltonian given by Eq. (3). Using a standard Jordan-Wigner transformation [67], the Ising chain [Eq. (3)] can be mapped into the free fermion Hamiltonian [Eq. (5)] with the identification $a_{3k} = 2\cos k$, $J = 1$, $g(t) = 2h(t) = 2(h_0 + h_1 \cos \omega_D t)$, and $\Delta_k = 2\sin k$. In this notation, the ferromagnetic state with spin-up on all sites is mapped to fermion vacuum. We note that such a transformation provides a direct relation between the fermion density operator $\hat{n}_j = c_j^\dagger c_j$ (where c_j denotes the fermion annihilation operator on site j) and σ_j^z as $\sigma_j^z = 1 - 2\hat{n}_j$.

We present our results obtained using both exact numerical computation of $U_k(T, 0)$ and using H_{Fk} [Eq. (12)] computed using second-order FPT. For the former, we follow the standard procedure of Suzuki-Trotter decomposition of U_k into n_0 steps of width $\delta t = T/n_0$. The width of these time steps are chosen such that $H_k(t)$ [Eq. (5)] does not change significantly within each of these steps. This allows one to numerically compute the evolution operator as

$$U_k(T, 0) = \prod_{j=1,n_0} U_k(t_j, t_{j-1}) = \prod_{j=1,n_0} e^{-i\delta t H_k(t_j)/\hbar}. \tag{24}$$

One can then diagonalize U_k to find out its eigenvalues $e^{i\theta_k^\pm}$ (where $\theta_k^\pm = E_k^\pm T/\hbar$ are in general complex numbers) and the corresponding eigenvectors $|\pm; k\rangle$. This leads to the evolution operator

$$U_k(nT, 0) = \sum_{a=\pm} e^{-in\theta_k^a} |a; k\rangle\langle a; k|. \tag{25}$$

Using Eq. (25) one can compute fidelity, correlation function, and entanglement entropy numerically following the steps outlined in Sec. II B

A. Floquet spectrum

In this subsection we present our results for the Floquet spectrum. To this end, we plot Γ_k and ϵ_k [Eq. (13)] in top panels of Fig. 1 for $\hbar\omega_D/J = 9.24$ [Fig. 1(a)] and 8 [Fig. 1(b)]. The branch of $E_k^\pm$ with $\epsilon_k > 0$ is plotted in Fig. 1. Both the figures show a change in sign of Γ_k around $k = k^* \sim 1.5$. The value of k^* is consistent with that found from the condition $k^* \simeq \arccos h_0$; this is due to the fact that the second-order

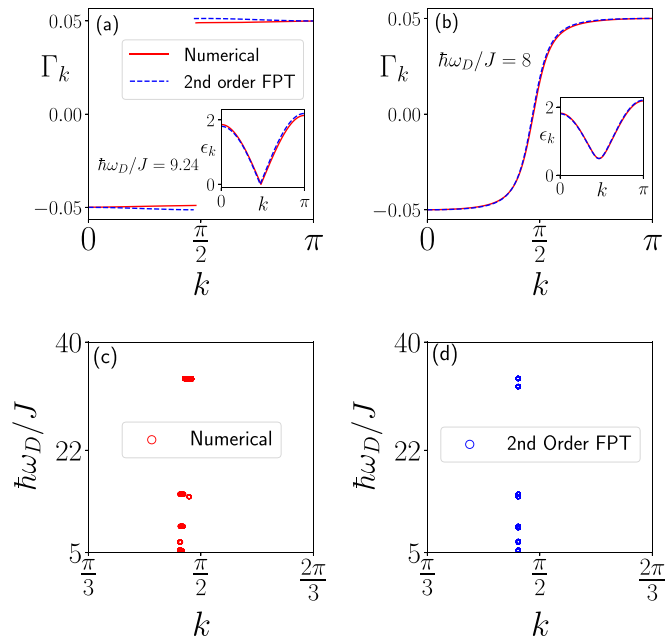

FIG. 1. (a) Plot of imaginary part of the spectrum Γ_k as a function of k for the branch having positive real part of the spectrum ($\epsilon_k > 0$) and with the drive frequency $\hbar\omega_D/J = 9.24$. The inset shows ϵ_k as a function of k. (b) Similar plot for $\hbar\omega_D/J = 8$. The red(blue) lines represents results obtained using exact numerics with system size $L = 1000$ (second-order FPT). (c) Plots of exceptional points as a function of $\hbar\omega_D/J$ and k as obtained using exact numerics. (d) Same as panel (c) as obtained from second-order FPT by solving Eq. (14). For all plots $h_0 = 0.1$, $\gamma = 0.05$, $h_1 = 20$ and energy scales are measured in units of J. See text for details.

contributions to the Floquet spectrum are small compared to the first-order terms. This shows that such a change in sign of Γ_k is contingent on the condition $|h_0| \leqslant 1$. The change of sign is gradual away from ω_m^* as shown for $\hbar\omega_D/J = 8$ in the right panel; in contrast, it is abrupt for $\hbar\omega_D/J = 9.24$ which corresponds to $\omega_D = \omega_3^*$. We have checked that a similar behavior holds near all other $\omega_D = \omega_m^*$. We also note that the second-order FPT (blue lines) shows an excellent match with the exact results (red lines) for all k. We shall use these properties of Γ_k, shown in Figs. 1(a) and 1(b), for the analysis of the properties of correlation functions and entanglement in the next section.

Figures 1(c) and 1(d) show the position of the exceptional points as a function of $\hbar\omega_D/J$ and k where both real and imaginary components of E_k vanishes. Figure 1(c) shows the positions of the exceptional points obtained from exact numerics; this is determined numerically by choosing $|E_k| \leqslant \delta$ where $\delta \sim 10^{-2}$. We have checked that lowering δ further does not change the nature of the plots. Figure 1(d) shows similar points obtained from second-order FPT by solving Eq. (14). We note that near the special frequencies where $J_0[4h_1/(\hbar\omega_D)] = 0$ leading to very small off-diagonal terms, our choice of parameters do not allow for exceptional point; this is clearly seen in Figs. 1(c) and 1(d). Moreover, such points form discrete set of points in k space; consequently, their presence do significantly affect the dynamics of magnetization or correlation functions which involves sum over all k points.

Before concluding this section, we note that the Floquet spectrum obtained from the second-order FPT matches quite well with exact numerics; moreover, the position of the exceptional points in the ω_D-k plane obtained by exact numerics also matches that obtained from Eq. (14). Thus, these results confirm the validity of second-order FPT for a wide range of ω_D.

B. Fidelity and correlations

In this section, we first study the fidelity $g(nT)$ [Eq. (20)] of the driven model as a function of n for several representative values of ω_D. These plots for fidelity are shown in Figs. 2(a) and 2(b) for an initial state $|\psi_0\rangle = \prod_k (u_{0k}, v_{0k})^T = \prod_k (0, 1)^T$ while Figs. 2(c) and 2(d) show analogous plots for $|\psi_0\rangle = \prod_k (1, 0)^T$ and $|\psi_0\rangle = \prod_k (1, 1)^T/\sqrt{2}$, respectively.

Figure 2(a) shows the behavior of $g(nT)$ for $\hbar\omega_D/J = 8$ and $\hbar\omega_D/J = 11$ (inset). These frequencies are far away from ω_m^* (for $m = 1, 2, 3...$) for which $J_0[4h_1/(\hbar\omega_D)] = 0$; thus, the behavior of $g(nT)$ in this plot represent its typical behavior for a ferromagnetic initial state at most frequencies. The plot indicates a decay of $g(nT)$ to its steady-state value with small but finite oscillations. These features are predicted by both second-order FPT (blue dashed lines) and exact numerics (red solid lines); the perturbative prediction match the exact results quite well at these frequencies.

In contrast, Figs. 2(b)–2(d) show the behavior of $g(nT)$ for $\hbar\omega_D/J = 9.24$ which corresponds to $\omega_D = \omega_3^*$. Figures 2(a) and 2(b) show lack of oscillations along with a steady-state value of $g(nT) \ll 0$. In contrast, the plot of $g(nT)$ in Fig. 2(c), which corresponds to an initial state $\prod_k (1, 0)^T$, yields a near-zero steady-state value. This indicates a high overlap of the steady state with the initial state. Figure 2(d), corresponding

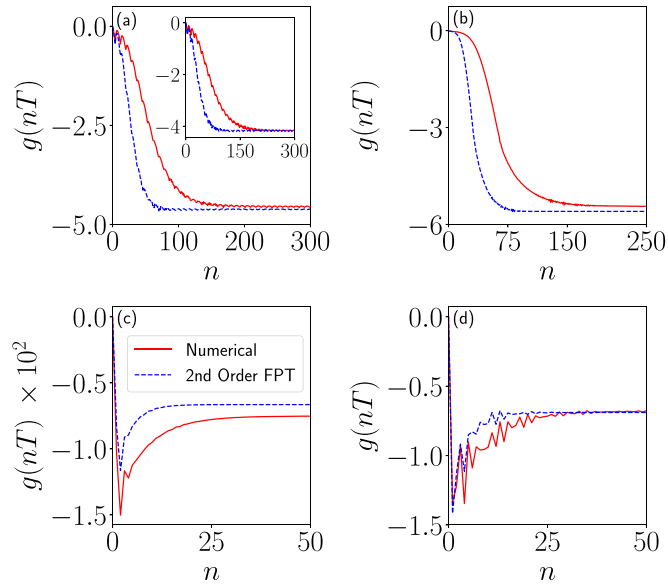

FIG. 2. (a) Plot of fidelity $g(nT)$ as a function of n for the drive frequency $\hbar\omega_D/J = 8$ and $|\psi_0\rangle = \prod_k (0, 1)^T$ which corresponds to the all spin-down ferromagnetic initial state. The inset shows analogous plot for $\hbar\omega_D/J = 11$. (b) Similar plot for $\hbar\omega_D/J = 9.24$. (c) Similar plot for $\hbar\omega_D/J = 9.24$ with the initial state $|\psi_0\rangle = \prod_k (1, 0)^T$ which corresponds to the all spin-up ferromagnetic state. (d) Similar plot for $\hbar\omega_D/J = 9.24$ with the initial state $|\psi_0\rangle = \prod_k (1, 1)^T/\sqrt{2}$. For all plots red (blue) represents results obtained from exact numerics (second-order FPT). All other parameters are same as in Fig. 1. See text for details.

to $|\psi_0\rangle = \prod_k (1, 1)^T/\sqrt{2}$, shows oscillatory nature of $g(nT)$ along with a steady-state value of $\sim \ln(1/2)$.

To qualitatively understand these features, we first consider the initial state $\prod_k (0, 1)^T$. For any given k, the wave function overlap for this initial state is given by $\chi_k(nT) = |v_k(nT)|^2$. Moreover, for this initial state, $\mu_{\pm k} = q_{\pm k}^*$ [Eq. (19)]. This leads to

$$\begin{aligned}\chi_k(nT) &= \frac{||q_{+k}|^2 e^{-iE_k nT/\hbar} + |q_{-k}|^2 e^{iE_k nT/\hbar}|^2}{|\mathcal{D}_k(\pi/2)|^2} \\ &= \frac{1}{\mathcal{D}_k^2(\pi/2)}\big[|q_{+k}|^4 e^{2\Gamma_k nT/\hbar} + |q_{-k}|^4 e^{-2\Gamma_k nT/\hbar} \\ &\quad + 2|q_{+k}q_{-k}|^2 \cos(2\epsilon_k nT/\hbar)\big], \end{aligned} \tag{26}$$

where we have used $E_k = \epsilon_k + i\Gamma_k$ and $\mathcal{D}_k(\pi/2) = \mathcal{D}_k(\theta_{0k} = \pi/2)$ [Eq. (19)]. The first two terms in the expression of χ_k determines its steady-state behavior while the last term yields the intermediate oscillation.

The nature of the fidelity can be qualitatively understood from the behavior of $q_{\pm k}$ and Γ_k as a function of k. The plots of $|p_{\pm k}|^2 = 1 - |q_{\pm k}|^2$ is shown in Fig. 3 as a function of k. From this plot, we note that near the special frequencies ω_m^*, $|q_{-k}|^2 \sim \theta(k - k^*)$ and $|q_{+k}|^2 \sim \theta(k^* - k)$; thus, the oscillations in $\chi_k(nT)$ whose amplitude $\sim |q_{+k}q_{-k}|^2$ vanishes for all n. Furthermore, when $nT|\Gamma_k|/\hbar \ll 1$, such that $\mathcal{D}_k(\pi/2) \sim (|q_{+k}|^2 + |q_{-k}|^2)^{1/2}$, we find

$$\chi_k \sim |q_{-k}|^2\theta(k - k^*) + |q_{+k}|^2\theta(k^* - k) \simeq 1. \tag{27}$$

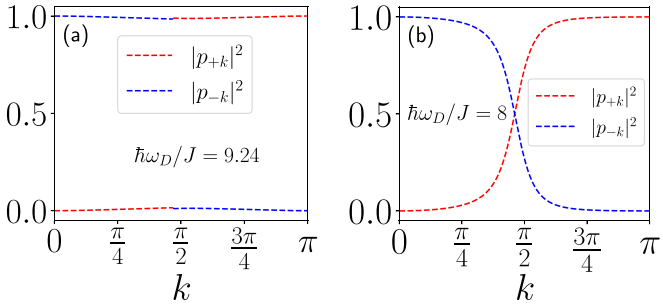

FIG. 3. Plot of coefficients $|p_{+k}|^2$ (red solid line) and $|p_{-k}|^2$ (blue solid line), obtained using second-order FPT, as a function k for $\hbar\omega_D/J = 9.24$ (a) and $\hbar\omega_D/J = 8$ (b). The behavior $q_{\pm k}$ can be read off from these plots using the relation $|p_{\pm k}|^2 + |q_{\pm k}|^2 = 1$. All other parameters are same as in Fig. 1. See text for details.

In contrast, for large n, where $nT|\Gamma_k|/\hbar \gg 1$, one has

$$\mathcal{D}_k^2(\pi/2) \simeq |q_{+k}|^2 \exp(2\Gamma_k nT/\hbar) + |q_{-k}|^2 \exp(-2\Gamma_k nT/\hbar), \tag{28}$$

the expression of χ_k can be written as

$$\chi_k \sim |q_{-k}|^2\left[1 + \left(\frac{|q_{+k}|e^{-|\Gamma_k|nT/\hbar}}{|q_{-k}|}\right)^4\right], \quad k < k^*,$$
$$\sim |q_{+k}|^2\left[1 + \left(\frac{|q_{-k}|e^{-|\Gamma_k|nT/\hbar}}{|q_{+k}|}\right)^4\right], \quad k > k^*, \tag{29}$$

where we have used the fact that $\Gamma_k < (>)0$ for $k < (>)k^*$ as shown in Figs. 1(a) and 1(b). This shows that $g(nT)$ [Eq. (20)] assumes a large negative value at large n; moreover, the decay to the steady state is exponential. The steady-state value of g depends on $\ln \chi_k$ for $nT|\Gamma_k|/\hbar \gg 1$; near $\omega = \omega_m^*$, where $q_{\pm k}$ shows a sharp jump around $k = k^*$, $\chi_k \sim |q_{\pm k}|^2 \to 0$ for all k as can be seen from Fig. 3. Thus, $g \sim \int dk \ln \chi_k$ assumes a large negative value as can be seen from Fig. 2(b)

For the initial state $\prod_k (1, 0)^T$, we find that $\mu_{\pm k} = p_{\pm k}^*$. Using this, a similar calculation yields

$$\chi_k(nT) = \frac{1}{\mathcal{D}_k^2(0)}\big[|p_{+k}|^4 e^{2\Gamma_k nT/\hbar} + |p_{-k}|^4 e^{-2\Gamma_k nT/\hbar} + 2|p_{+k}p_{-k}|^2 \cos(2\epsilon_k nT/\hbar)\big]. \tag{30}$$

We note that near ω_m^* for $|\Gamma_k|nT/\hbar \ll 1$, a similar analysis as given in Eq. (27) yields $\chi_k \sim 1$. In contrast, for the steady state where $|\Gamma_k|nT/\hbar \gg 1$, we find

$$\chi_k \sim |p_{-k}|^2\left[1 + \frac{|p_{+k}|^4 \exp(-4|\Gamma_k|nT/\hbar)}{|p_{-k}|^4}\right], \quad k < k^*,$$
$$\sim |p_{+k}|^2\left[1 + \frac{|p_{-k}|^4 \exp(-4|\Gamma_k|nT/\hbar)}{|p_{+k}|^4}\right], \quad k > k^*. \tag{31}$$

Thus, the steady-state value of χ_k remains close to unity for all k near ω_m^* (Fig. 3). Consequently $g(nT) \sim 0$. Our analysis thus reveals the reason of small values of $g(nT)$ when one start from the initial state $\prod_k (1, 0)^T$; this also results in a slightly lower match of $g(nT)$ obtained from second-order FPT with its exact numerical counterpart since the finite value of g in this case comes mostly from higher-order terms in the perturbation series. We note that the oscillations are absent for all n since the amplitude of such oscillations depends on $|p_{+k}p_{-k}|^2$ and is vanishingly small for all k.

Finally, for the initial state $\prod_k (1, 1)^T/\sqrt{2}$, we find $\mu_{\pm k} = (p_{\pm k}^* + q_{\pm k}^*)/\sqrt{2}$. Using this, one obtains

$$\chi_k(nT) = \frac{1}{\mathcal{D}_k^2(\pi/4)}\Big\{\sum_{s=\pm}\big[|R_{sk}|^2 e^{2s\Gamma_k nT/\hbar}\big] + 2R_{+k}R_{-k}\cos(2\epsilon_k nT/\hbar)\Big\},$$
$$R_{sk} = \frac{1}{2}[1 + (p_{sk}^* q_{sk} + \text{H.c.})]. \tag{32}$$

We note that at large n, this yields

$$\chi_k \sim R_{-k}\left[1 + \left(\frac{R_{+k}e^{-2|\Gamma_k|nT/\hbar}}{R_{-k}}\right)^2\right], \quad k < k^*,$$
$$\sim R_{+k}\left[1 + \left(\frac{R_{-k}e^{-2|\Gamma_k|nT/\hbar}}{R_{+k}}\right)^2\right], \quad k > k^*. \tag{33}$$

For $\omega_D = \omega_m^*$, $p_{sk}^* q_{sk} \simeq 0$ for all k leading $R_{\pm k} \sim 1/2$ (Fig. 3). Thus, the steady-state value of $\chi_k \sim 1/2$ for all k; this leads to a $g \simeq -\ln 2$ in the steady state. The other features of $g(nT)$ can be inferred from an analysis similar to those carried out for $\theta_{0k} = 0, \pi/2$. Thus, our analysis of $g(nT)$ as shown in Fig. 2 indicates that the presence of special frequencies ω_m^* shapes the nature of the fidelity of the driven system.

The nature of the steady state of the driven non-Hermitian steady state can be further understood by studying the steady-state value of the magnetization of the driven system. We note first that the magnetization of the driven Ising chain is given by

$$M(nT) = -\int_0^\pi \frac{dk}{\pi} N_k(nT) = \int_0^\pi \frac{dk}{\pi}(1 - 2|v_k(nT)|^2). \tag{34}$$

The steady-state value of the magnetization, M^{st}, is obtained for $n \gg \text{Min}[J/\Gamma_k]$. Using Eqs. (19), and starting from an initial product state $\prod_k (0, 1)^T$, which corresponds to $M(0) = -1$, we find that

$$N_k(nT) = \frac{-1}{\mathcal{D}_k^2(\pi/2)}\Big\{\sum_{s=\pm}\big[|q_{sk}|^2(|p_{sk}|^2 - |q_{sk}|^2)e^{2s\Gamma_k nT/\hbar}\big] + 2\text{Re}\big[q_{+k}q_{-k}^*(p_{+k}^* p_{-k} - q_{+k}^* q_{-k})e^{2i\epsilon_k nT/\hbar}\big]\Big\}. \tag{35}$$

For $|\Gamma_k|nT/\hbar \gg 1$, since Γ_k changes sign at $k = k^*$, the steady-state value of N_k, N_k^{st}, is given terms of $p_{\pm k}$, $q_{\pm k}$ by

$$N_k^{\text{st}} = (|q_{-k}|^2 - |p_{-k}|^2)\big(1 - \eta_{0k}e^{-4|\Gamma_k|nT/\hbar}\big), \quad k < k^*,$$
$$= (|q_{+k}|^2 - |p_{+k}|^2)\big(1 - \eta_{0k}^{-1}e^{-4|\Gamma_k|nT/\hbar}\big), \quad k > k^*,$$
$$\eta_{0k} = \frac{(|q_{+k}|^2 - |p_{+k}|^2)}{(|p_{-k}|^2 - |q_{-k}|^2)}\frac{|q_{+k}|^2}{|q_{-k}|^2}. \tag{36}$$

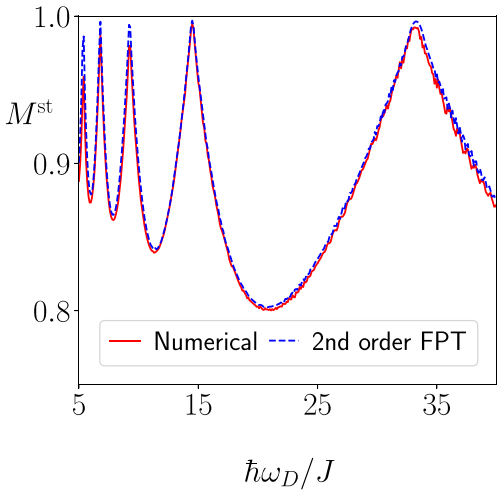

FIG. 4. Plot of $M^{\rm st}$ as a function $\hbar\omega_D/J$ as obtained from exact numerics and second-order FPT. All parameters are same as in Fig. 1. See text for details.

Thus, when $\omega_D \sim \omega_m^*$, $N_k^{\rm st} \sim -1$ for all k leading to a steady-state magnetization $M^{\rm st} \sim 1$. However, away from these frequencies, both $p_{\pm k}$ and $q_{\pm k}$ are finite around $k = k^*$; thus, the value of $N_k^{\rm st}$ deviates from -1 when k is within this range. This in turn leads to lower value of $M^{\rm st}$ when ω_D is away from ω_m^*. We therefore expect nonmonotonic behavior of $M^{\rm st}$ as a function of the drive frequency.

The plot of the steady $M^{\rm st}$, obtained from the value of $M(nT)$ around $n \sim 1000$ after averaging over 50 drive cycles, plotted as a function of ω_D in Fig. 4 (red curve), conforms this behavior. The plot clearly shows that the steady-state magnetization exhibits distinct dips at $\omega_D = \omega_m^*$. The blue curve of Fig. 4 shows the plot of $M^{\rm st}$ as obtained from second-order perturbation theory. Here the steady state is constructed, for each k, from the normalized wave function $|\psi_k(nT)\rangle$ [Eq. (18)] by retaining terms in $u_k(nT)$ and $v_k(nT)$ [Eq. (19)] with $\Gamma_k > 0$ which survive in the limit $n \to \infty$. This yields $u_k^{\rm st}$ and $v_k^{\rm st}$ and leads to $M^{\rm st} = \int_0^\pi (dk/\pi)(1 - 2|v_k^{\rm st}|^2)$. The result obtained from second-order FPT in this manner is remarkably close to the exact result. Thus, we conclude that the steady state of the driven chain bears the signature of the approximate dynamical symmetry as shown in Fig. 4.

Next, we study the behavior of the magnetization $M(nT)$ [Eq. (34)] as a function of n and the drive frequency ω_D. The corresponding plot is shown in Fig. 5. Figure 5(a) shows the behavior of $M(nT)$ obtained from exact numerics, while Fig. 5(b) shows the corresponding results from second-order FPT; the latter shows excellent match with the former for a wide range of drive frequencies. The behavior of $M(nT)$ shown in these plots can be understood from Eq. (35) as follows.

First, we note that near ω_m^*, the oscillatory terms in Eq. (35) vanishes since $p_{sk}q_{sk} \sim 0$ for $s = \pm$ and all k. Thus, we expect the oscillatory behavior of $M(nT)$ to be present only away from these frequencies. This behavior is confirmed by plots in Fig. 5. Second, from Fig. 5, we find that at $\omega_D = \omega_m^*$, M stays close to its initial value for a large number of drive cycles; this is followed by a sharp decay to the

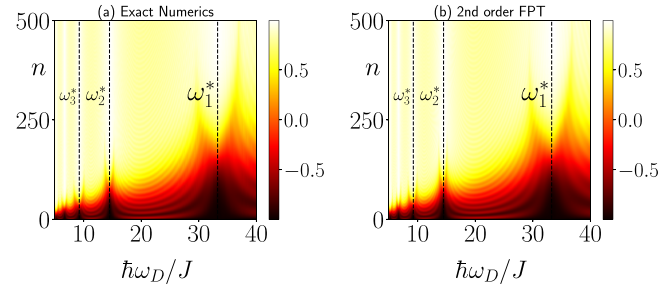

FIG. 5. Plot of the magnetization $M(nT)$ as a function of the number of drive cycles n and the drive frequency $\hbar\omega_D/J$ as obtained from exact numerics (a) and second-order FPT (b). All parameters are same as in Fig. 1. See text for details.

steady-state value $M^{\rm st} \simeq 1$. The sharpness of this decay is a consequence of sharp change of $q_{\pm k}$ and Γ_k around $k = k^*$. Third, the deviation of M from the steady-state value occurs when $\eta_{0k}^{-1}(\eta_{0k})\exp[-4|\Gamma_k|n_cT/\hbar] \sim 1$ for $k > (<)k^*$ [Eq. (36)]. Thus, the value of n_c at which this crossover occurs is exponentially sensitive to the distribution of $|\Gamma_k|$ as a function of k around $k = k^*$. Since a sharp change of sign of Γ_k around $k = k^*$, which occurs around ω_m^*, indicates a larger value of $|\Gamma_k|$ for most k, we find that the system reaches its steady state for smallest value of n_c at ω_m^*. As one moves away from ω_m^*, n_c increases; concomitantly, $q_{\pm k}$ develop finite value for larger range of k around k^*. Thus, $M(nT)$ starts to change with n for $n < n_c$ in an oscillatory manner. The oscillation amplitude are small near ω_m^*; thus, the system shows very slow change in magnetization in the region $0 \leqslant n \leqslant n_c$. This leads to peaklike structures around ω_m^* (Fig. 5) where the systems shows slow but nonzero change in the magnetization before reaching the steady state.

Next, we study the off-diagonal fermion correlation function $F(nT)$ given by

$$F(nT) = \int_0^\pi \frac{dk}{\pi} F_k(nT). \tag{37}$$

The plot of $F(nT)$ as a function of n and $\hbar\omega_D/J$ is shown in Fig. 6. Once again we find that the second-order FPT [Fig. 6(b)] reproduces all the qualitative features obtained using exact numerics [Fig. 6(a)]. To understand these features, we first note that starting from an initial state $\prod_k (0, 1)^T$, the

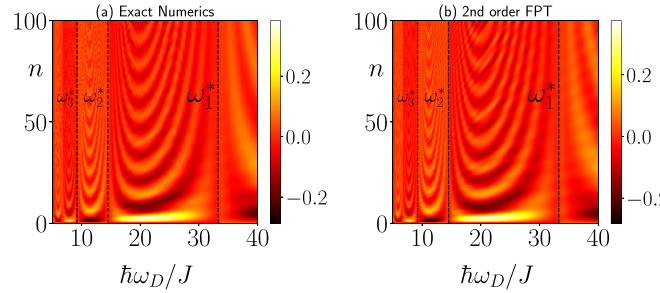

FIG. 6. Plot of the correlation function $F(nT)$ as a function of the number of drive cycles n and drive frequency $\hbar\omega_D/J$ as obtained from exact numerics (a) and second-order FPT (b). All parameters are same as in Fig. 1. See text for details.

expression of $F_k(nT)$ can be written terms of $p_{\pm k}$ and $q_{\pm k}$ as

$$F_k(nT) = \frac{2}{\mathcal{D}_k^2(\pi/2)} \sum_{s=\pm} (|q_{sk}|^2 \mathrm{Re}[p_{sk}^* q_{sk}] e^{2s\Gamma_k nT/\hbar} + |q_{-sk}|^2 \times \{\mathrm{Re}[p_{sk}^* q_{sk}] \cos(2\epsilon_k nT/\hbar) - s\mathrm{Im}[p_{sk}^* q_{sk}] \times \sin(2\epsilon_k nT/\hbar)\}). \quad (38)$$

From Eq. (38), we find that $F_k \sim 0$ for all k at ω_m^* since $|p_{sk}^* q_{sk}| \sim 0$ for $s = \pm$ and at all k at these frequencies. The amplitude of the oscillations of $F_k(nT)$ is also small for the same reason. Consequently, $F(nT)$ remains close to zero at these frequencies for all n. In contrast, significant oscillations are seem away from ω_m^* where both p_{sk} and q_{sk} are finite for a range of k around k^*. Thus, our analysis of $M(nT)$ and $F(nT)$, as shown in Figs. 5 and 6, respectively, indicates that their properties can serve as a tool for detecting the magic frequencies ω_m^*.

To summarize, we find that all correlations and the fidelity bear signature of the approximate dynamical symmetry that emerges at ω_m^*. The footprint of this emergent symmetry constitutes lack of oscillatory features in fidelity and correlation functions which can be discerned most easily by measuring magnetization of the driven chain.

C. Entanglement

In this section we present our results for entanglement entropy of the driven system. In what follows, we shall mostly concentrate on the half-chain Von-Neumann entropy $S_{\ell=L/2}(nT) \equiv S(nT)$ [Eq. (23)], where L is the chain length, as a function of n and ω_D.

A plot of $S(nT)$ is shown, starting from an initial state $|\psi_0\rangle = \prod_k (0, 1)^T$, as a function of n and ω_D in Fig. 7. The plots show that S follows an almost similar pattern as the correlation functions and hence bears a signature of the special frequencies. Moreover, from these plots, we find, comparing Figs. 7(a) and 7(b), that the second-order FPT matches well with exact numerics for a wide range of drive frequency.

The plot of S as a function of n for a fixed drive frequency $\hbar\omega_D/J = 8$ is shown in Fig. 7(c). The behavior of S, as shown in this plot, brings out a key difference between it and its counterpart for driven Hermitian Ising chains [28]. For periodically driven Hermitian chains, S is known to first increase and then saturate with increasing n. In contrast, for a driven non-Hermitian chain S first increases, reaches a peak, and then decays to its steady-state value at large n. This behavior can be understood as follows.

The initial state of the system $|\psi_0\rangle$ is a product state leading to $S(0) = 0$. For small n, the behavior of S shows a similar increase as in Hermitian driven chain. However, for large n where $|\Gamma_k|nT/\hbar \geqslant 1$ for all k, it starts to approach its steady-state value. In contrast to driven Hermitian chains, the steady state here has a low entropy, being an almost product state. This indicates that $S(nT)$ for large n is also small; in fact, it approaches zero as $\omega_D \to \omega_m^*$ where the steady state is a perfect product state with $S = 0$. This ensures that $S(nT)$ is necessarily a nonmonotonic function of n. In between, $S(nT)$ reaches its peak value; the position of this peak depends on both ω_D and γ. We note that these features of $S(nT)$ are accurately captured by the second-order FPT [blue curve in Fig. 7(c)] which provides a near-exact match with exact numerical results [red curve in Fig. 7(c)]. We note that Figs. 7(a) and 7(b) indicate that the behavior of $S(nT)$ near $\omega_D = \omega_m^*$ is qualitatively different compared to that away from ω_m^*.

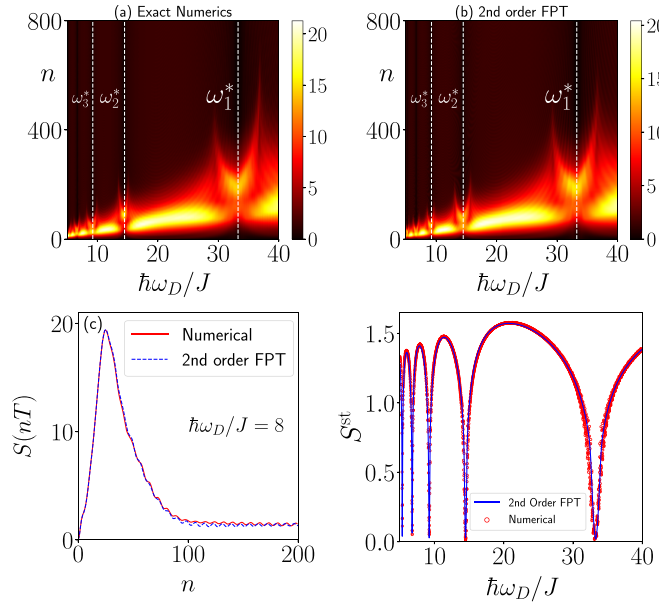

FIG. 7. Plot of the entanglement $S(nT)$ as a function of the number of drive cycles n and the drive frequency $\hbar\omega_D/J$ as obtained from exact numerics (a) and second-order FPT (b). (c) Plot of $S(nT)$ as a function of n for $\hbar\omega_D/J = 8$. (d) Plot of the steady-state entanglement S^{st} as a function of ω_D showing dips at $\omega_D = \omega_m^*$. For panels (c) and (d) red (blue) lines circles (lines) represent results obtained from exact numerics (second-order FPT). We have chosen $L = 100$ for all plots; the rest of the parameters are same as in Fig. 1. See text for details.

The behavior of $S(nT)$ for $\omega_D = \omega_m^*$ as a function of n is qualitatively similar to that shown in Fig. 7(c) with two important differences. First, the oscillatory features of S are absent at these frequencies, and second, the steady-state value of S approaches zero. The latter can be most easily inferred from the plot of S^{st} as a function of ω_D as shown in Fig. 7(d). We find that the special frequencies ω_m^* can be distinguished by dips in S^{st}; this can be understood as a consequence of the fact that the steady state, at these frequencies, are very close to the product state $|\psi_s\rangle = \prod_k (1, 0)^T$. This confirms that the steady-state entanglement, shown in Fig. 7(d), also bears the signature of the emergent approximate conservation.

IV. DISCUSSION

In this work, we have studied a class of driven 1D non-Hermitian integrable free fermionic models in the high drive-amplitude regime. We have identified the presence of approximately conserved quantities that leave their imprints on the dynamics of these models. We have shown in the Appendix that such emergent conservation can also be seen for discrete drive protocols; this demonstrates the general, protocol-independent, nature of this phenomenon.

For a continuous drive protocol, we have used Floquet perturbation theory to obtain the Floquet Hamiltonian H_F of the driven models. The method uses inverse of the drive amplitude

as the perturbation parameter and thus provides reasonably accurate results for high and intermediate drive frequency regimes. This distinguishes it from the standard high frequency expansions where the inverse frequency is taken as the perturbation parameter. We show, using the example of 1D transverse field Ising chain, that the dynamics obtained using H_F computed from second-order FPT reproduces all the features of its exact numerical counterpart.

The Floquet Hamiltonian obtained using this method provides analytic understanding of the reason for the emergent approximate conservation at special frequencies. At these frequencies, whose analytic expressions can be obtained using FPT, the first-order Floquet Hamiltonian (also obtained from FPT) commutes with certain operators. A specific example of such an operator is shown to correspond to the transverse magnetization of the driven non-Hermitian Ising chain. Such a conservation is approximate and it is shown to be violated by higher (second) order Floquet Hamiltonian. Nevertheless, this approximate emergent conservation leaves its signature on the dynamics of the driven chain. In this respect, non-Hermitian systems differ qualitatively from their Hermitian counterparts studied in Refs. [77]; for example, the magnetization of the latter stays very close to its initial value for a very large number of drive cycles at such special drive frequencies. In contrast, the magnetization of integrable non-Hermitian systems studied here exhibit distinct dynamics and approaches its steady-state value after $n \sim 200$ drive cycles.

We discus the dynamical signature of this approximate conservation and show that it also shapes the nature of the steady states of these driven systems. Using the Ising model in a transverse field as an example, we show that the steady state of the driven non-Hermitian Ising chain coincides with an eigenstate of the transverse magnetization at these special frequencies. Moreover, the approach of the system to the steady state shows distinct behavior at these special frequencies; they lack the transient oscillations which is normally present when the drive frequency is away from these special frequencies. Such a qualitatively different behavior is also reflected in the entanglement entropy S of such systems. In particular, for the Ising chain, the steady-state entanglement entropy $S^{\rm st}$ approaches zero at these special frequencies; in contrast, it is finite at other drive frequencies. Our study also indicates the nonmonotonic behavior of S as a function of n and ties it to the non-Hermitian nature of these models.

There have been several suggestions of realization of non-Hermitian Ising chains [72–75]. Some of these protocols involve coupling a Hermitian Ising chain with a continuously measuring device which measures the transverse magnetization; the effective Hamiltonian of the system in the so-called no-click limit is then given by a Ising chain with an imaginary component γ_0 of the transverse field [65]. The net transverse field acting on the Ising spin thus becomes $B + i\gamma_0$, where B denotes the existing transverse field of the uncoupled Hermitian Ising chain. Our proposition is to drive the chain with a time dependent magnetic field $B = B_0 + B_1 \cos \omega_D t$ starting from an all-down spin state. In the limit of large drive amplitude, we predict that the steady-state magnetization per unit length of the chain would be close to $\hbar/2$ at special drive frequencies $\omega_D = \omega_m^*$. These frequencies are predicted to be related to the drive amplitude by $h_1/(\hbar\omega_m^*) = \rho_m$ where ρ_m denotes the position of the $m^{\rm th}$ zero of J_0 and $h_1 = \mu_0 B$ where μ_0 is the magnetic moment associated with the Ising spins. A similar phenomenon would be seen for square pulse protocol at $h_1/(\hbar\omega_m^*) = m\pi$. The approach of the magnetization $M(nT)$ to its steady-state value $M^{\rm st}$ as a function of the number of drive cycles n can also be measured; we predict that the evolution of $M(nT)$ will be consistent with Fig. 5 and it will show lack of transient oscillations for $\omega_D = \omega_m^*$.

In conclusion, we have studied the Floquet dynamics of a class of driven non-Hermitian integrable models. We have identified special drive frequencies in these systems which leads to emergence of approximate conservation laws. We have identified the signature of this phenomenon in the dynamics of the driven systems and suggested experiments which can test our theory.

ACKNOWLEDGMENTS

K.S. thanks DST, India for support through SERB Project No. JCB/2021/000030.

APPENDIX: SQUARE PULSE PROTOCOL

In this Appendix, we show the presence of approximate conservation laws in the limit of high drive amplitude for integrable non-Hermitian free-fermionic models for a square pulse protocol. To this end, we consider a square pulse drive protocol

$$\begin{aligned} g(t) &= g_0 \quad \text{for } t \leqslant T/2 \\ &= -g_0 \quad \text{for } t > T/2, \end{aligned} \tag{A1}$$

where T is the time period. Substituting Eq. (A1) in Eq. (2), one finds the evolution operator of the system at $t = T$ and for a given $\vec{k}$ to be

$$\begin{aligned} U_{\vec{k}}^{\rm sq}(T,0) &= e^{-iH_{\vec{k}}^- T/(2\hbar)} e^{-iH_{\vec{k}}^+ T/(2\hbar)}, \\ H_{\vec{k}}^{\pm} &= (\pm g_0 - a_{3\vec{k}} + i\gamma)\tau_3 + \Delta_{\vec{k}}\tau_1. \end{aligned} \tag{A2}$$

A straightforward analysis yields

$$\begin{aligned} U_{\vec{k}}^{\rm sq} &= \begin{pmatrix} \alpha_1 & \beta_1 \\ \beta_2 & \alpha_2 \end{pmatrix}, \\ \alpha_j &= [\cos\theta_{\vec{k}}^+ + i(-1)^j n_{3\vec{k}}^+ \sin\theta_{\vec{k}}^+][\cos\theta_{\vec{k}}^- + i(-1)^j n_{3\vec{k}}^- \sin\theta_{\vec{k}}^-] - n_{1\vec{k}}^+ n_{1\vec{k}}^- \sin\theta_{\vec{k}}^+ \sin\theta_{\vec{k}}^-, \\ \beta_j &= -i\{n_{1\vec{k}}^+ \sin\theta_{\vec{k}}^+ [\cos\theta_{\vec{k}}^- + i(-1)^j n_{3\vec{k}}^- \sin\theta_{\vec{k}}^-] + n_{1\vec{k}}^- \sin\theta_{\vec{k}}^- [\cos\theta_{\vec{k}}^+ - i(-1)^j n_{3\vec{k}}^+ \sin\theta_{\vec{k}}^+]\}, \\ n_{1\vec{k}}^{\pm} &= \frac{\Delta_{\vec{k}}}{E_{\vec{k}}^{\pm}}, \quad n_{3\vec{k}}^{\pm} = \frac{\pm g_0 - a_{3\vec{k}} + i\gamma}{E_{\vec{k}}^{\pm}}, \quad E_{\vec{k}}^{\pm} = \sqrt{(\pm g_0 - a_{3\vec{k}} + i\gamma)^2 + \Delta_{\vec{k}}^2}, \quad \theta_{\vec{k}}^{\pm} = E_{\vec{k}}^{\pm} T/(2\hbar). \end{aligned} \tag{A3}$$

Equation (A3) yields exact $U_{\vec{k}}$ for any drive frequency and amplitude. Now we note that for large drive amplitude $g_0 \gg a_{3\vec{k}}, \Delta_{\vec{k}}, \gamma$, the off-diagonal terms of $U_{\vec{k}}(T,0)$ vanish for special drive frequencies $g_0/\omega_m^* = m$ where $m \in Z$. For these frequencies, $[\tau_3, U_{\vec{k}}(T,0)] = 0$ (to leading order in $1/g_0$) for all $\vec{k}$ leading to approximate conservation which is violated only in subleading order in $1/g_0$. This violation is hence small in the large g_0 limit. This demonstrates the presence of special frequencies for the square pulse drive protocol.

[1] A. Polkovnikov, K. Sengupta, A. Silva, and M. Vengalattore, Rev. Mod. Phys. **83**, 863 (2011).

[2] J. Dziarmaga, Adv. Phys. **59**, 1063 (2010).

[3] A. Dutta, G. Aeppli, B. K. Chakrabarti, U. Divakaran, T. F. Rosenbaum, and D. Sen, *Quantum Phase Transitions in Transverse Field Spin Models: From Statistical Physics to Quantum Information* (Cambridge University Press, Cambridge, UK, 2015).

[4] S. Mondal, D. Sen, and K. Sengupta, *Quantum Quenching, Annealing and Computation*, edited by A. Das, A. Chandra, and B. K. Chakrabarti, Lecture Notes in Physics Vol. 802 (Springer, Berlin, 2010), p. 21; C. De Grandi and A. Polkovnikov, *ibid.* Vol. 802, p. 75.

[5] A. del Campo and K. Sengupta, Eur. Phys. J. Spec. Top. **224**, 189 (2015).

[6] M. Bukov, L. D'Alessio, and A. Polkovnikov, Adv. Phys. **64**, 139 (2015).

[7] L. D'Alessio and A. Polkovnikov, Ann. Phys. **333**, 19 (2013).

[8] L. D'Alessio, Y. Kafri, A. Polokovnikov, and M. Rigol, Adv. Phys. **65**, 239 (2016).

[9] A. Sen, D. Sen, and K. Sengupta, J. Phys.: Condens. Matter **33**, 443003 (2021).

[10] M. Greiner, O. Mandel, T. Esslinger, T. W. Hansch, and I. Bloch, Nature (London) **415**, 39 (2002).

[11] J. Simon, W. S. Bakr, R. Ma, M. E. Tai, P. M. Preiss, and M. Greiner, Nature (London) **472**, 307 (2011)

[12] W. Bakr, A. Peng, E. Tai, R. Ma, J. Simon, J. Gillen, S. Foelling, L. Pollet, and M. Greiner, Science **329**, 547 (2010).

[13] H. Bernien, S. Schwartz, A. Keesling, H. Levine, A. Omran, H. Pichler, S. Choi, A. S. Zibrov, M. Endres, M. Greiner, V. Vuletic, and M. D. Lukin, Nature (London) **551**, 579 (2017).

[14] S. Geier, N. Thaicharoen, C. Hainaut, T. Franz, A. Salzinger, A. Tebben, D. Grimshandl, G. Zurn, and M. Weidemuller, Science **374**, 1149 (2021); P. Scholl, H. J. Williams, G. Bornet, F. Wallner, D. Barredo, L. Henriet, A. Signoles, C. Hainaut, T. Franz, S. Geier, A. Tebben, A. Salzinger, G. Zurn, T. Lahaye, M. Weidemuller, and A. Browaeys, PRX Quantum **3**, 020303 (2022); P. Peng, C. Yin, X. Huang, C. Ramanathan, and P. Cappellaro, Nat. Phys. **17**, 444 (2021).

[15] S. Blanes, F. Casas, J. A. Oteo, and J. Ros, Phys. Rep. **470**, 151 (2009).

[16] T. Oka and H. Aoki, Phys. Rev. B **79**, 081406(R) (2009).

[17] T. Kitagawa, E. Berg, M. Rudner, and E. Demler, Phys. Rev. B **82**, 235114 (2010); N. H. Lindner, G. Refael, and V. Galitski, Nat. Phys. **7**, 490 (2011).

[18] T. Kitagawa, T. Oka, A. Brataas, L. Fu, and E. Demler, Phys. Rev. B **84**, 235108 (2011); B. Mukherjee, P. Mohan, D. Sen, and K. Sengupta, *ibid.* **97**, 205415 (2018).

[19] M. Thakurathi, A. A. Patel, D. Sen, and A. Dutta, Phys. Rev. B **88**, 155133 (2013); A. Kundu, H. A. Fertig, and B. Seradjeh, Phys. Rev. Lett. **113**, 236803 (2014); K. Sengupta and M. Thakurathi, Phys. Rev. B **89**, 235434 (2014).

[20] F. Nathan and M. S. Rudner, New J. Phys. **17**, 125014 (2015); B. Mukherjee, A. Sen, D. Sen, and K. Sengupta, Phys. Rev. B **94**, 155122 (2016).

[21] V. Khemani, A. Lazarides, R. Moessner, and S. L. Sondhi, Phys. Rev. Lett. **116**, 250401 (2016).

[22] D. V. Else, B. Bauer, and C. Nayak, Phys. Rev. Lett. **117**, 090402 (2016).

[23] J. Zhang, P. W. Hess, A. Kyprianidis, P. Becker, A. Lee, J. Smith, G. Pagano, I.-D. Potirniche, A. C. Potter, A. Vishwanath, N. Y. Yao, and C. Monroe, Nature (London) **543**, 217 (2017).

[24] B. Mukherjee, S. Nandy, A. Sen, D. Sen, and K. Sengupta, Phys. Rev. B **101**, 245107 (2020).

[25] B. Mukherjee, A. Sen, D. Sen, and K. Sengupta, Phys. Rev. B **102**, 075123 (2020).

[26] B. Mukherjee, A. Sen, and K. Sengupta, Phys. Rev. B **106**, 064305 (2022).

[27] M. Heyl, A. Polkovnikov, and S. Kehrein, Phys. Rev. Lett. **110**, 135704 (2013); for a review, see M. Heyl, Rep. Prog. Phys. **81**, 054001 (2018).

[28] A. Sen, S. Nandy, and K. Sengupta, Phys. Rev. B **94**, 214301 (2016); S. Nandy, K. Sengupta, and A. Sen, J. Phys. A: Math. Theor. **51**, 334002 (2018); M. Sarkar and K. Sengupta, Phys. Rev. B **102**, 235154 (2020).

[29] S. Aditya, S. Samanta, A. Sen, K. Sengupta, and D. Sen, Phys. Rev. B **105**, 104303 (2022); A. A. Makki, S. Bandyopadhyay, S. Maity, and A. Dutta, *ibid.* **105**, 054301 (2022); S. E. Tapias Arze, P. W. Clayes, I. P. Castillo, and J.-S. Caux, SciPost Phys. Core **3**, 001 (2020).

[30] T. Nag, S. Roy, A. Dutta, and D. Sen, Phys. Rev. B **89**, 165425 (2014); T. Nag, D. Sen, and A. Dutta, Phys. Rev. A **91**, 063607 (2015).

[31] A. Agarwala, U. Bhattacharya, A. Dutta, and D. Sen, Phys. Rev. B **93**, 174301 (2016); A. Agarwala and D. Sen, *ibid.* **95**, 014305 (2017).

[32] D. J. Luitz, Y. Bar Lev, and A. Lazarides, SciPost Phys. **3**, 029 (2017); D. J. Luitz, A. Lazarides, and Y. Bar Lev, Phys. Rev. B **97**, 020303(R) (2018).

[33] A. Das, Phys. Rev. B **82**, 172402 (2010).

[34] S. Bhattacharyya, A. Das, and S. Dasgupta, Phys. Rev. B **86**, 054410 (2012).

[35] S. S. Hegde, H. Katiyar, T. S. Mahesh, and A. Das, Phys. Rev. B **90**, 174407 (2014).

[36] S. Mondal, D. Pekker, and K. Sengupta, Europhys. Lett. **100**, 60007 (2012).

[37] U. Divakaran and K. Sengupta, Phys. Rev. B **90**, 184303 (2014).

[38] For a recent review of non-Hermitian topological phenomena, see N. Okuma and M. Sato, Ann. Rev. Cond. Mat. **14**, 83 (2023).

[39] J. Gonzalez and R. A. Molina, Phys. Rev. B **96**, 045437 (2017); V. Kozii and L. Fu, arXiv:1708.05841; A. A. Zyuzin and A. Y. Zyuzin, Phys. Rev. B **97**, 041203 (2018); H. Shen and L. Fu, Phys. Rev. Lett. **121**, 026403 (2018); R. A. Molina and J. Gonzalez, *ibid.* **120**, 146601 (2018); T. Yoshida, R. Peters, and

N. Kawakami, Phys. Rev. B **98**, 035141 (2018); J. Carlström and E. J. Bergholtz, Phys. Rev. A **98**, 042114 (2018).

[40] T. M. Philip, M. R. Hirsbrunner, and M. J. Gilbert, Phys. Rev. B **98**, 155430 (2018); Y. Chen and H. Zhai, *ibid.* **98**, 245130 (2018); K. Moors, A. A. Zyuzin, A. Y. Zyuzin, R. P. Tiwari, and T. L. Schmidt, *ibid.* **99**, 041116(R) (2019); R. Okugawa and T. Yokoyama, *ibid.* **99**, 041202(R) (2019); J. C. Budich, J. Carlstrom, F. K. Kunst, and E. J. Bergholtz, *ibid.* **99**, 041406(R) (2019).

[41] Z. Yang and J. Hu, Phys. Rev. B **99**, 081102(R) (2019); T. Yoshida, R. Peters, N. Kawakami, and Y. Hatsugai, *ibid.* **99**, 121101(R) (2019); Y. Wu, W. Liu, J. Geng, X. Song, X. Ye, C.-K. Duan, X. Rong, and J. Du, Science **364**, 878 (2019); P. San-Jose, J. Cayao, E. Prada, and R. Aguado, Sci. Rep. **6**, 21427 (2016); Q.-B. Zeng, B. Zhu, S. Chen, L. You, and R. Lu, Phys. Rev. A **94**, 022119 (2016); C. Li, X. Z. Zhang, G. Zhang, and Z. Song, Phys. Rev. B **97**, 115436 (2018); J. Cayao and A. M. Black-Schaffer, *ibid.* **105**, 094502 (2022); R. Arouca, J. Cayao, and A. M. Black-Schaffer, arXiv:2206.15324.

[42] K. Kawabata, Y. Ashida, H. Katsura, and M. Ueda, Phys. Rev. B **98**, 085116 (2018); A. Guo, G. J. Salamo, D. Duchesne, R. Morandotti, M. Volatier-Ravat, V. Aimez, G. A. Siviloglou, and D. N. Christodoulides, Phys. Rev. Lett. **103**, 093902 (2009); C. E. Rüter, K. G. Makris, R. El-Ganainy, D. N. Christodoulides, M. Segev, and D. Kip, Nat. Phys. **6**, 192 (2010); L. Feng, M. Ayache, J. Huang, Y.-L. Xu, M.-H. Lu, Y.-F. Chen, Y. Fainman, and A. Scherer, Science **333**, 729 (2011); A. Regensburger, C. Bersch, M.-A. Miri, G. Onishchukov, D. N. Christodoulides, and U. Peschel, Nature (London) **488**, 167 (2012).

[43] L. Feng, Y.-L. Xu, W. S. Fegadolli, M.-H. Lu, J. E. Oliveira, V. R. Almeida, Y.-F. Chen, and A. Scherer, Nat. Mater. **12**, 108 (2013); C. Poli, M. Bellec, U. Kuhl, F. Mortessagne, and H. Schomerus, Nat. Commun. **6**, 6710 (2015); B. Zhen, C. W. Hsu, Y. Igarashi, L. Lu, I. Kaminer, A. Pick, S.-L. Chua, J. D. Joannopoulos, and M. Solja, Nature (London) **525**, 354 (2015); H. Zhao, S. Longhi, and L. Feng, Sci. Rep. **5**, 17022 (2015); K. Ding, Z. Q. Zhang, and C. T. Chan, Phys. Rev. B **92**, 235310 (2015).

[44] S. Weimann, M. Kremer, Y. Plotnik, Y. Lumer, S. Nolte, K. Makris, M. Segev, M. Rechtsman, and A. Szameit, Nat. Mater. **16**, 433 (2017); H. Hodaei, A. U. Hassan, S. Wittek, H. Garcia-Gracia, R. El-Ganainy, D. N. Christodoulides, and M. Khajavikhan, Nature (London) **548**, 187 (2017); W. Chen, K. Ozdemir, G. Zhao, J. Wiersig, and L. Yang, *ibid.* **548**, 192 (2017); P. St-Jean, V. Goblot, E. Galopin, A. Lemaitre, T. Ozawa, L. Le Gratiet, I. Sagnes, J. Bloch, and A. Amo, Nat. Photonics **11**, 651 (2017).

[45] B. Bahari, A. Ndao, F. Vallini, A. E. Amili, Y. Fainman, and B. K. Le, Science **358**, 636 (2017); J. Wang, H. Y. Dong, Q. Y. Shi, W. Wang, and K. H. Fung, Phys. Rev. B **97**, 014428 (2018); H. Zhou, C. Peng, Y. Yoon, C. W. Hsu, K. A. Nelson, L. Fu, J. D. Joannopoulos, M. Solja, and B. Zhen, Science **359**, 1009 (2018); M. Parto, S. Wittek, H. Hodaei, G. Harari, M. A. Bandres, J. Ren, M. C. Rechtsman, M. Segev, D. N. Christodoulides, and M. Khajavikhan, Phys. Rev. Lett. **120**, 113901 (2018); H. Zhao, P. Miao, M. H. Teimourpour, S. Malzard, R. El-Ganainy, H. Schomerus, and L. Feng, Nat. Commun. **9**, 981 (2018).

[46] G. Harari, M. A. Bandres, Y. Lumer, M. C. Rechtsman, Y. D. Chong, M. Khajavikhan, D. N. Christodoulides, and M. Segev, Science **359**, 1230 (2018); M. A. Bandres, S. Wittek, G. Harari, M. Parto, J. Ren, M. Segev, D. N. Christodoulides, and M. Khajavikhan, *ibid.* **359**, 1231 (2018); M. Pan, H. Zhao, P. Miao, S. Longhi, and L. Feng, Nat. Commun. **9**, 1308 (2018); L. Jin and Z. Song, Phys. Rev. Lett. **121**, 073901 (2018); S. Malzard and H. Schomerus, Phys. Rev. A **98**, 033807 (2018); Z. Oztas and C. Yuce, *ibid.* **98**, 042104 (2018).

[47] M. Kremer, T. Biesenthal, L. J. Maczewsky, M. Heinrich, R. Thomale, and A. Szameit, Nat. Commun. **10**, 435 (2019); K. Y. Bliokh, D. Leykam, M. Lein, and F. Nori, *ibid.* **10**, 580 (2019); S. Wang, B. Hou, W. Lu, Y. Chen, Z. Zhang, and C. Chan, *ibid.* **10**, 832 (2019); S. Chen, W. Zhang, B. Yang, T. Wu, and X. Zhang, Sci. Rep. **9**, 5551 (2019); Y. Xu, S.-T. Wang, and L.-M. Duan, Phys. Rev. Lett. **118**, 045701 (2017); Y. Ashida, S. Furukawa, and M. Ueda, Nat. Commun. **8**, 15791 (2017); Z. Gong, Y. Ashida, K. Kawabata, K. Takasan, S. Higashikawa, and M. Ueda, Phys. Rev. X **8**, 031079 (2018); M. Nakagawa, N. Kawakami, and M. Ueda, Phys. Rev. Lett. **121**, 203001 (2018); K. Takata and M. Notomi, *ibid.* **121**, 213902 (2018); L. Pan, S. Chen, and X. Cui, Phys. Rev. A **99**, 011601(R) (2019).

[48] J. Li, A. K. Harter, J. Liu, L. de Melo, Y. N. Joglekar, and L. Luo, Nat. Commun. **10**, 855 (2019); T. Liu, Y.-R. Zhang, Q. Ai, Z. Gong, K. Kawabata, M. Ueda, and F. Nori, Phys. Rev. Lett. **122**, 076801 (2019); M. S. Rudner and L. S. Levitov, *ibid.* **102**, 065703 (2009); J. M. Zeuner, M. C. Rechtsman, Y. Plotnik, Y. Lumer, S. Nolte, M. S. Rudner, M. Segev, and A. Szameit, *ibid.* **115**, 040402 (2015); K. Mochizuki, D. Kim, and H. Obuse, Phys. Rev. A **93**, 062116 (2016); L. Xiao, X. Zhan, Z. Bian, K. Wang, X. Zhang, X. Wang, J. Li, K. Mochizuki, D. Kim, N. Kawakami *et al.*, Nat. Phys. **13**, 1117 (2017).

[49] N. Hatano and D. R. Nelson, Phys. Rev. Lett. **77**, 570 (1996); Phys. Rev. B **56**, 8651 (1997); **58**, 8384 (1998).

[50] J. A. S. Lourenço, R. L. Eneias, and R. G. Pereira, Phys. Rev. B **98**, 085126 (2018); E. I. Rosenthal, N. K. Ehrlich, M. S. Rudner, A. P. Higginbotham, and K. W. Lehnert, *ibid.* **97**, 220301(R) (2018); M. Wang, L. Ye, J. Christensen, and Z. Liu, Phys. Rev. Lett. **120**, 246601 (2018).

[51] M. Ezawa, Phys. Rev. B **99**, 121411(R) (2019); **99**, 201411(R) (2019); **100**, 045407 (2019).

[52] M. Prasad, H. K. Yadalam, C. Aron, and M. Kulkarni, Phys. Rev. A **105**, L050201 (2022).

[53] E. Lee, H. Lee, and B.-J. Yang, Phys. Rev. B **101**, 121109(R) (2020); S. Mu, C. H. Lee, L. Li, and J. Gong, *ibid.* **102**, 081115(R) (2020); D.-W. Zhang, Y.-L. Chen, G.-Q. Zhang, L.-J. Lang, Z. Li, and S.-L. Zhu, *ibid.* **101**, 235150 (2020); T. Liu, J. J. He, T. Yoshida, Z.-L. Xiang, and F. Nori, *ibid.* **102**, 235151 (2020).

[54] A. Panda and S. Banerjee, Phys. Rev. B **101**, 184201 (2020); N. Okuma and M. Sato, Phys. Rev. Lett. **126**, 176601 (2021); T. Yoshida, Phys. Rev. B **103**, 125145 (2021); K. Cao, Q. Du, X.-R. Wang, and S.-P. Kou, arXiv:2109.03690; F. Alsallom, L. Herviou, O. V. Yazyev, and M. Brzezinska, Phys. Rev. Res. **4**, 033122 (2022).

[55] S-B Zhang, S.-B. Zhang, Tomas Bzdusek, M. A. Sentef, and T. Neupert, Phys. Rev. B **106**, L121102 (2022).

[56] Y. C. Hu and T. L. Hughes, Phys. Rev. B **84**, 153101 (2011); K. Esaki, M. Sato, K. Hasebe, and M. Kohmoto, *ibid.* **84**, 205128 (2011); T. E. Lee, Phys. Rev. Lett. **116**, 133903 (2016); D. Leykam, K. Y. Bliokh, C. Huang, Y. D. Chong, and F. Nori, *ibid.* **118**, 040401 (2017); V. M. Martinez Alvarez, J. E. Barrios Vargas, and L. E. F. Foa Torres, Phys. Rev. B **97**, 121401(R) (2018); Y. Xiong, J. Phys. Commun. **2**, 035043 (2018); H. Shen, B. Zhen, and L. Fu, Phys. Rev. Lett. **120**, 146402 (2018).

[57] C. Yuce, Phys. Rev. A **97**, 042118 (2018); C. Yin, H. Jiang, L. Li, R. Lu, and S. Chen, *ibid.* **97**, 052115 (2018); C. Yuce, *ibid.* **98**, 012111 (2018); F. K. Kunst, E. Edvardsson, J. C. Budich, and E. J. Bergholtz, Phys. Rev. Lett. **121**, 026808 (2018); S. Yao and Z. Wang, *ibid.* **121**, 086803 (2018); S. Yao, F. Song, and Z. Wang, *ibid.* **121**, 136802 (2018); K. Kawabata, K. Shiozaki, and M. Ueda, Phys. Rev. B **98**, 165148 (2018); C. Yuce and Z. Oztas, Sci. Rep. **8**, 17416 (2018).

[58] K. Kawabata, S. Higashikawa, Z. Gong, Y. Ashida, and M. Ueda, Nat. Commun. **10**, 297 (2019); L. Jin and Z. Song, Phys. Rev. B **99**, 081103(R) (2019); H. Wang, J. Ruan, and H. Zhang, **99**, 075130 (2019); D. S. Borgnia, A. J. Kruchkov, and R.-J. Slager, Phys. Rev. Lett. **124**, 056802 (2020); Z. Ozcakmakli Turker and C. Yuce, Phys. Rev. A **99**, 022127 (2019); E. Edvardsson, F. K. Kunst, and E. J. Bergholtz, Phys. Rev. B **99**, 081302(R) (2019).

[59] C.-H. Liu, H. Jiang, and S. Chen, Phys. Rev. B **99**, 125103 (2019); C. H. Lee and R. Thomale, *ibid.* **99**, 201103(R) (2019); F. K. Kunst and V. Dwivedi, *ibid.* **99**, 245116 (2019); K. Yokomizo and S. Murakami, Phys. Rev. Lett. **123**, 066404 (2019).

[60] R. Nehra and D. Roy, Phys. Rev. B **105**, 195407 (2022); K. Kawabata, K. Shiozaki, and S. Ryu, *ibid.* **105**, 165137 (2022); K. Yang, D. Varjas, E. J. Bergholtz, S. Morampudi, and F. Wilczek, ApJ **928**, 33 (2022).

[61] L. Zhou, Q.-h. Wang, H. Wang, and J. Gong, Phys. Rev. A **98**, 022129 (2018); L. Zhou and Q. Du, New J. Phys. **23**, 063041 (2021); B. Zhu, Y. Ke, H. Zhong, and C. Lee, Phys. Rev. Res. **2**, 023043 (2020); L. Zhou and J. Gong, Phys. Rev. B **98**, 205417 (2018); L. Zhou, *ibid.* **100**, 184314 (2019); L. Zhou, Y. Gu, and J. Gong, *ibid.* **103**, L041404 (2021).

[62] L. Zhou and W. Han, Phys. Rev. B **106**, 054307 (2022); C.-H. Liu and S. Chen, *ibid.* **105**, 214305 (2022); L. Zhou, R. W. Bomantara, and S. Wu, SciPost Phys. **13**, 015 (2022).

[63] S. Zamani, R. Jafari, and A. Langari, Phys. Rev. B **102**, 144306 (2020); R. Jafari and A. Akbari, Phys. Rev. A **103**, 012204 (2021); K. Yang, L. Zhou, W. Ma, X. Kong, P. Wang, X. Qin, X. Rong, Y. Wang, F. Shi, J. Gong, and J. Du, Phys. Rev. B **100**, 085308 (2019); D. Chowdhury and A. Banerjee, and A. Narayan, Phys. Rev. A **103**, L051101 (2021).

[64] P. He and Z.-H. Huang, Phys. Rev. A **102**, 062201 (2020); S. Longhi, J. Phys. A: Math. Theor. **50**, 505201 (2017).

[65] X. Turkeshi and M. Schiro, Phys. Rev. B **107**, L020403 (2023).

[66] J. Ren, P. Hanggi, and B. Li, Phys. Rev. Lett. **104**, 170601 (2010); J. Ren, S. Liu, and B. Li, *ibid.* **108**, 210603 (2012); H. Xu, D. Mason, L. Jiang, and J. G. E. Harris, Nature (London) **537**, 80 (2016); Z. Wang, J. Chen, and J. Ren, Phys. Rev. E **106**, L032102 (2022); L. J. Fernández-Alcazar, R. Kononchuk, H. Li, and T. Kottos, Phys. Rev. Lett. **126**, 204101 (2021).

[67] S. Sachdev, *Quantum Phase Transitions*, 2nd ed. (Cambridge University Press, Cambridge, UK, 2011).

[68] A. H. Castro Neto, F. Guinea, N. M. R. Peres, and K. S. Novoselov, and A. K. Geim, Rev. Mod. Phys. **81**, 109 (2009).

[69] M. Z. Hasan and C. L. Kane, Rev. Mod. Phys. **82**, 3045 (2010).

[70] A. Kitaev, Ann. Phys. **321**, 2 (2006).

[71] N. P. Armitage, E. J. Mele, and A. Vishwanath, Rev. Mod. Phys. **90**, 015001 (2018).

[72] J. Dalibard, Y. Castin, and K. Molmer, Phys. Rev. Lett. **68**, 580 (1992).

[73] A. J. Daley, Adv. Phys. **63**, 77 (2014).

[74] T. E. Lee and C.-K. Chan, Phys. Rev. X **4**, 041001 (2014).

[75] J. Pi and R. Lu, J. Phys.: Condens. Matter **33**, 345601 (2021).

[76] S. Sharma, A. Russomanno, G. Santoro, and A. Dutta, Europhys. Lett. **106**, 67003 (2014).

[77] A. Haldar, R. Moessner, and A. Das, Phys. Rev. B **97**, 245122 (2018); A. Haldar, D. Sen, R. Moessner, and A. Das, Phys. Rev. X **11**, 021008 (2021); C. Yin, P. Peng, X. Huang, C. Ramanathan, and P. Cappellaro, Phys. Rev. B **103**, 054305 (2021).